Fly motion vision is based on Reichardt detectors regardless of the signal-to-noise ratio

J. Haag*, W. Denk†, and A. Borst*‡

*Max Planck Institute of Neurobiology, D-82152 Martinsried, Germany; and †Max Planck Institute for Medical Research, D-69120 Heidelberg, Germany

Communicated by Bert Sakmann, Max Planck Institute for Medical Research, Heidelberg, Germany, October 6, 2004 (received for review May 19, 2004)

The computational structure of an optimal motion detector was proposed to depend on the signal-to-noise ratio (SNR) of the stimulus: At low SNR, the optimal motion detector should be a correlation or ''Reichardt'' type, whereas at high SNR, the detector would employ a gradient scheme [Potters, M. & Bialek, W. (1994) *J. Physiol. (Paris)* 4, 1755–1775]. Although a large body of experiments supports the Reichardt detector as the processing scheme leading to direction selectivity in fly motion vision, in most of these studies the SNR was rather low. We therefore reinvestigated the question over a much larger SNR range. Using 2-photon microscopy, we found that local dendritic [Ca^{2+}] modulations, which are characteristic of Reichardt detectors, occur in response to drifting gratings over a wide range of luminance levels and contrasts. We also explored, as another fingerprint of Reichardt detectors, the dependence of the velocity optimum on the pattern wavelength. Again, we found Reichardt-typical behavior throughout the whole luminance and contrast range tested. Our results, therefore, provide strong evidence that only a single elementary processing scheme is used in fly motion vision.

calcium imaging | computational model | motion detection

In motion vision, two distinct models have been proposed to account for direction selectivity: the Reichardt detector and the gradient detector (Fig. 1). In the Reichardt detector (also called Hassenstein–Reichardt detector or correlation-type motion detector), the luminance levels of two neighboring image locations are multiplied after being filtered asymmetrically (Fig. 1*a*). This operation is performed twice in a mirror-symmetrical fashion before the outputs of both multipliers are subtracted from one another (1–4). The spatial or temporal average of such local motion detector signals is proportional to the image velocity within a range set by the detector time constant (5). It is one of the hallmarks of this model, however, that the output of the individual velocity detectors depends on the spatial structure of the moving pattern (in addition to the stimulus velocity) in a characteristic way. In response to drifting gratings, for example, the local Reichardt detector output consists of two components: a sustained [direct current (DC)] component, which indicates by its sign the direction of the moving stimulus, and an alternating current (AC) component, which follows the local intensity modulation and, thus, carries no directional information at all. Because the local intensity modulations are phase-shifted with respect to each other, the AC components in the local signals are cancelled by the spatial integration of many adjacent detectors. Unlike the AC component, the DC component survives spatial or temporal averaging (integration). The global output signal, therefore, is purely directional. It is predicted to exhibit a distinct optimum as a function of stimulus velocity for each pattern wavelength. The ratio of velocity and spatial wavelength at this optimum corresponds to a certain temporal frequency, which is the number of spatial pattern periods passing one particular image location each second. Despite having a different internal structure, the so-called "energy model" (6) is identical to the Reichardt detector with respect to the output signal (7) and, consequently, with respect to all of the above predictions (for review see ref. 8). The energy model will, therefore, not be treated as a separate model here.

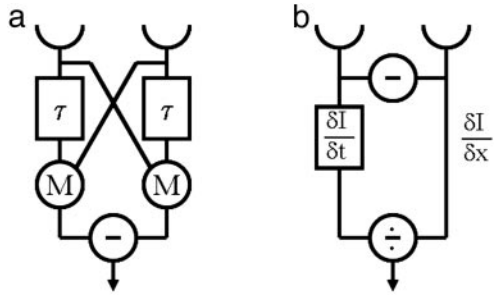

Fig. 1. Two competing mechanisms proposed to underlie direction selectivity in fly motion detection. (*a*) The Reichardt detector consists of two mirror-symmetrical subunits. In each subunit, the luminance values as measured in two adjacent image locations become multiplied (M) with each other after one of them is delayed by a low-pass filter with time-constant τ. The resulting output signals of the multipliers become finally subtracted. (*b*) In the gradient detector, the temporal luminance gradient as measured after one photoreceptor ($\delta I/\delta t$, *Left*) is divided by the spatial luminance gradient ($\delta I/\delta x$). Here, the spatial gradient is approximated by the difference between the luminance values in two adjacent image locations. According to the central hypothesis being tested in this study, the mechanism should switch over from *a* to *b* with an increasing SNR in the stimulus.

The "gradient detector" model is a prominent alternative model for motion detection (9–12). The gradient detector computes the velocity signal by dividing the temporal derivative of local luminance $\partial I(x,t)/\partial t$ by its spatial derivative $\partial I(x,t)/\partial x$ (Fig. 1*b*). In contrast to the Reichardt detector, the gradient detector provides a signal that is proportional to image velocity at each point and does not depend on pattern properties. In particular, with the gradient detector, no modulations are expected in the local signals as long as the velocity is constant, and the velocity dependence of the global signal should not vary with the spatial wavelength of the pattern. The principal problem with the computation performed by the gradient detector is that the uncertainty in the computed velocity varies widely. If the spatial derivative $\partial I(x,t)/\partial x$ is small, the noise in the temporal derivative is amplified, and for points where the spatial derivative is zero, the velocity is completely undefined. To compensate for this problem, Potters and Bialek (13) proposed that an ideal motion scheme would be based on the gradient detector only in the high signal-to-noise regime, whereas at low signal-to-noise ratios (SNRs), a Reichardt detector would be superior.

Many studies of the mechanisms underlying direction selectivity have been performed on the fly visual system. There, large, motion-sensitive neurons are found in the lobula plate that spatially pool the output signals on their dendrites from many thousands of directionally selective neurons (Fig. 2*a*). According to the terminology introduced in the previous paragraph, therefore, the axonal signals of these neurons represent the global detector signal in the

Freely available online through the PNAS open access option.

Abbreviations: SNR, signal-to-noise ratio; DC, direct current; AC, alternating current.

‡To whom correspondence should be addressed. E-mail: borst@neuro.mpg.de.

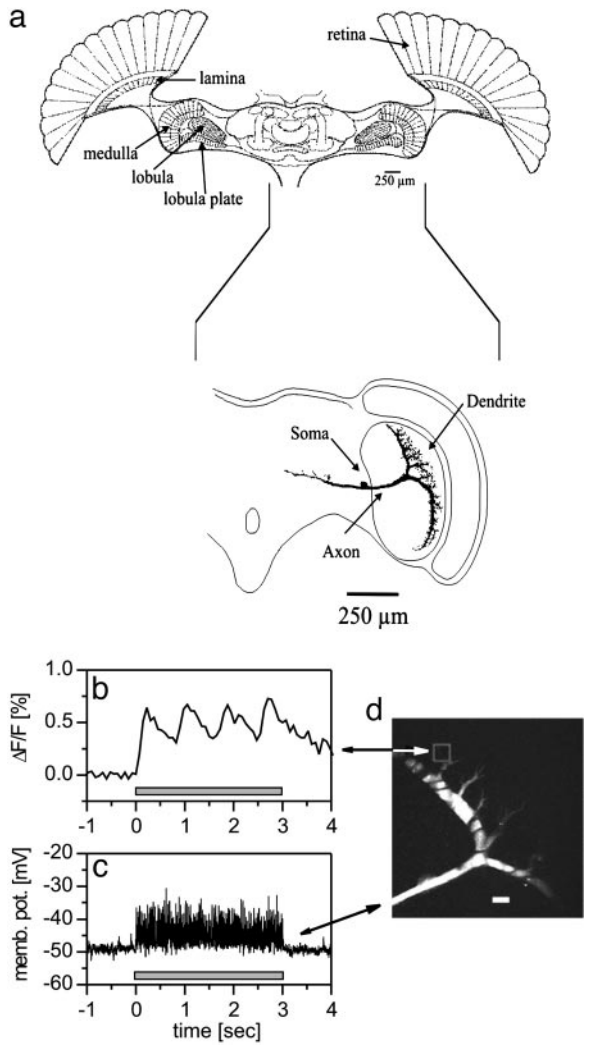

Fig. 2. Sample recording from a motion-sensitive neuron in the lobula plate (VS2 cell). (*a*) Schematic outline of the fly's head ganglion (*Upper*, horizontal view; *Lower*, enlarged frontal view). Visual information from the eyes is processed retinotopically in three successive layers called the lamina, the medulla, and the lobula complex, the latter being divided into an anterior lobula and a posterior lobula plate. In the lobula plate, large tangential cells spatially integrate the output of local motion-sensitive elements. As an example, one of these cells, a VS2 cell, is depicted here. Note that information flows from the dendrite to the axon bypassing the soma which is connected to the axon only through a thin, cell-body fiber. (*b*) Fluorescence signal is shown during motion along the preferred direction of the cell. Fluorescence was stimulated at 850 nm. Measurements were taken from the VS2 cell shown in *d* within the indicated area (red box). (*c*) Membrane potential is recorded simultaneously from the axon of the cell (indicated by the arrow). Unlike the local dendritic signal, no modulation is visible because of spatial integration over many periodic signals, which are phase-shifted with respect to each other in different dendritic areas. (*d*) Projected 2-photon image stack ("extended focus"). (Scale bar: 20 μm.) Stimulus parameters: mean luminance of 50,000 cd/m^2, contrast of 98%, spatial pattern wavelength of 8.3°, stimulus velocity of 10.8°/s, and temporal frequency of 1.3 Hz.

fly visual system. To examine the local detector signals in this system, ideally, one would record from local columnar units providing input to these cells; however, the small diameter of their processes prohibits intracellular recording. The same holds true for the fine dendritic endings of the lobula plate tangential cells. As an alternative, previous investigations of this problem resorted to optical recordings of free cytosolic calcium levels that can be accomplished after loading a fluorescent calcium indicator into the cell via intracellular electrodes into one of the larger processes of the tangential cell. Upon stimulation of the cell, calcium enters tangential cells through voltage-dependent and transmitter-gated channels and, therefore, qualifies well as a reporter of electrical activity (14–18).

By using this approach, previous measurements of [Ca^{2+}] in the dendritic tips of integrating motion-sensitive neurons revealed local modulations upon stimulation by uniformly moving gratings (19). These modulations were synchronous with the temporal frequency of the moving pattern and phase-shifted with respect to each other in different parts of the dendrite, thus providing clear evidence in favor of Reichardt-type motion processing (as previously described) in the fly visual system. However, because of the inevitable, spurious stimulation of photoreceptors that occurs during 1-photon imaging (20), the pattern contrast as seen by the fly, and therefore the SNR level, was rather low in those experiments, leaving open the possibility that, in a parameter region not reachable by those experiments, a different neural processing scheme might be used. This possibility has been suggested by Potters and Bialek (13). Spurious stimulation of photoreceptors can be virtually eliminated, however, by using 2-photon microscopy where excitation is limited to the focus volume. Resolution along the *z* axis not only eliminates stimulation of the photoreceptors by the excitation light, but also improves z-resolution and allows efficient detection of fluorescence light (21).

Strong evidence for the Reichardt model and against the gradient detector had also been provided by behavioral measurements of the fly optomotor response (22, 23) showing that the optimal stimulus velocity increased with pattern wavelength. Again, however, apart from one study (24), mean luminance levels were rather low, leaving room for alternative interpretations (see above). Therefore, in the second part of *Results*, we report a series of experiments on the fly motion-sensitive neuron H1 in which we tested the dependence of the optimal stimulus velocity on the pattern wavelength over a wide range of mean luminance levels and stimulus contrasts.

To summarize, the hypothesis being tested is that with increasing SNR of the stimulus, the motion processing scheme shifts from the Reichardt to the gradient detector model (13). If the hypothesis is true, we expect to see modulations in the local signal to decrease with increasing SNR. Furthermore, we expect to see a constant temporal frequency optimum for different spatial wavelengths in the global signal at low SNRs that will increasingly sort out with rising SNR levels. We manipulate the signal-to-noise level in the input in two different ways. In one case, we vary the mean luminance. Given the Poisson distribution of photon emission, the SNR grows with the square root with increasing luminance. In the other case, we vary the pattern contrast. For a peak-to-peak comparison, the signal, and hence the SNR, grows linearly with the contrast. In brief, the findings presented in the following do not support the above hypothesis.

Materials and Methods

Preparation. Female blowflies were briefly anesthetized with CO_2 and mounted with wax ventral side up on a small preparation platform. The head capsule was opened from behind; and the trachea and air sacs, which normally cover the lobula plate, were removed. For intracellular recordings (see *Pattern Dependence of the Local Detector Signals*), the proboscis of the animal was cut away and the gut was pulled out to eliminate movements of the brain caused by peristaltic contractions of the esophagus. Thus, stable intracellular recordings were possible for up to 1 h. For extracellular recordings of H1 neuron spikes (see *Pattern Dependence of the Integrated Detector Output*), the proboscis and the gut were left intact.

Cell Labeling. For electrophysiological recordings and intracellular injection of the [Ca^{2+}] indicator (Ca-Green I hexapotassium, Molecular Probes), electrodes were pulled on a Brown–Flaming

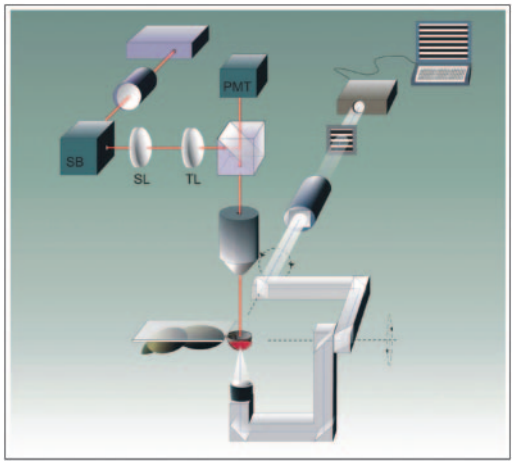

Fig. 3. Schematic drawing of the setup used for 2-photon [Ca^{2+}] imaging and visual stimulation *in vivo*. The fly is shown under an objective lens, looking down into an eyepiece mounted on a swivel arm that can be revolved around two axes (dashed lines). From the top, the femtosecond laser pulse excites the fluorophore in the visual interneuron with the emitted photons being collected by a photomultiplier. On the right side, the stimulus light path is shown: A moving grating is generated by a computer and fed through a dove prism into the optics leading to the eyepiece. SB, scan box; SL, scan lens; TL, tube lens; PMT, photomultiplier tube.

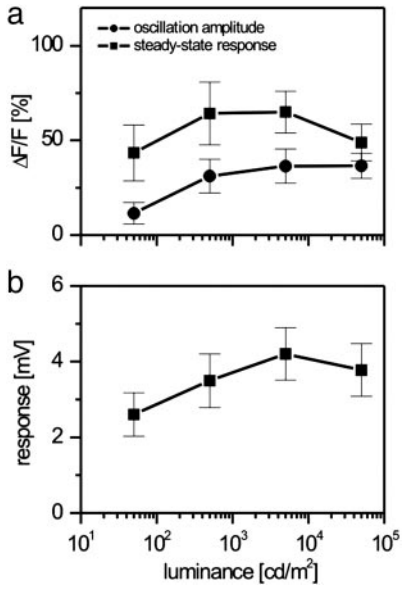

Fig. 4. Luminance dependence of motion responses. (*a*) Local [Ca^{2+}] signals of VS and HS cells. The response consists of a steady-state elevation of the [Ca^{2+}] signal superimposed by temporal oscillations. The two signal parts are plotted independently as a function of the mean stimulus luminance. (*b*) Average membrane depolarization during preferred direction motion is shown as a function of mean stimulus luminance. Values represent the mean ± SEM from measurements on 11 different flies.

micropipette puller (P-97, Sutter Instruments, Novato, CA) by using thin-wall glass capillaries with an outer diameter of 1 mm (GC100TF-10, Clark, WPI, Sarasota, FL). When filled with 2 M KAc/0.5 M KC/8.8 mM Ca-Green, they had resistances of ≈30–40 MΩ. Cells were labeled by applying a hyperpolarizing current of 3 nA for ≈5 min. A SEC-10L amplifier (NPI Instruments, Tamm, Germany) was used in bridge or discontinuous current clamp mode throughout the experiments. Fluorescence was 2-photon excited at 850 nm.

Principles of [Ca^{2+}] Imaging in the Visual System. There are two problems to be solved: The epifluorescence excitation light coming from above must not interfere with the fly's vision process, and the visual stimulus light falling in the fly's eye has to be kept from entering the optics leading to the photomultiplier tubes (Fig. 3). The first problem can be eliminated satisfactorily by using 2-photon microscopy (25) in which pulsed infrared light is used to cause 2-photon excitation. Because of quadratic intensity dependency, infrared light is largely confined to the focal region and thereby provides strong optical sectioning during excitation. This approach has been used successfully for [Ca^{2+}] recordings in the mammalian retina (26, 27). The absence of photoreceptor activation, even by intense infrared light shone into the back of the fly's head, was confirmed by using electrophysiological recordings in which no membrane voltage change was seen in response to opening the shutter of the 2-photon excitation laser. To avoid generating a false signal in the fluorescence channel, one needs to prevent the stimulus light from reaching the photodetector (in our case a photomultiplier tube). This can be achieved by using appropriate nonoverlapping wavelength filters for fluorescence and stimulation light. We used a short-pass filter, thereby limiting the spectral range of the stimulus light to <450 nm. The remaining short-wavelength light stimulates the photoreceptors strongly enough because the fly photo pigments are UV-sensitive (28). In order not to tax the finite blocking ability of the filters, it is helpful to concentrate the stimulus light as much as possible. This can be achieved as follows (Fig. 3). Instead of looking at a screen onto which the visual pattern is projected, the fly looks at the pattern through an eyepiece with the eye point (the illumination aperture) at the center of the eye's surface curvature. This technique minimizes scattered photons and ensures that light from the stimulus path is entering the fly visual system very efficiently.

Instrumentation for Two-Photon Imaging. We used a custom-built 2-photon microscope (29) and stimulation device (Fig. 3). Briefly, the microscope consists of the following components: a 5-W pumped Ti:Sapphire laser (MaiTai, Spectra-Physics; some of the early experiments in Heidelberg were carried out with a Mira 900/Verdi 10 combination), a pockels cell (Conoptics, Danbury, CT), scan mirrors including drivers (Cambridge Technology, Cambridge, MA), a scan lens (4401-302, Rodenstock, Munich), a tube lens (MXA 22018, Nikon), a dichroic mirror (DCSPR 25.5 × 36, AHF, Tuebingen, Germany), and a ×40 water immersion lens (Zeiss). The lens can move along all three axes by a step-motor-driven micromanipulator (MP285-3Z, Sutter Instruments, Novato, CA). Emitted light is filtered by a bandpass (HQ 535/50, Chroma Technology, Rockingham, VT) and collected by a multialkali photomultiplier (R6357, Hamamatsu Photonics, Hamamatsu City, Japan). Visual stimuli are provided by a computer via a video projector (MP7770, 3M Co.), filtered by a short-pass (10SWF-450, Newport, Irvine, CA), and focused by a total of three lenses in the path. The image can be rotated around the fly in two axes by means of step motors (Owis, Staufen, Germany). The whole system is controlled by custom-written software. In the experiments reported here, mean luminance was varied over 3 orders of magnitude by means of neutral density filters. The visual angle subtended by the grating amounted to 0.1 steradian, stimulating ≈300 ommatidia. The grating had a wavelength of 8.6° and was moved at a velocity of 10.8°/s, resulting in a temporal frequency of 1.3 Hz.

Evaluation of Optical Data. Images were taken at 64 × 64 pixel resolution at a frame rate of ≈8 Hz (128 ms per frame). These image series were evaluated off-line by using custom-written software (IDL, Research Systems, Boulder, CO). After transforming the images into fluorescence changes relative to the first image, a function consisting of a variable DC level and a sinusoid of 1.3 Hz with variable phase and amplitude was least-mean-square-fitted to

the data from each cell. The parameter values obtained in this way were subsequently averaged (Figs. 4*a* and 5*d*).

H1 Recordings. The H1 neuron was stimulated by a periodic grating moving at a constant velocity for 5 s, followed by a pause of 3 s during which the pattern was at rest. The pattern moved always in the direction preferred by the H1 neuron, i.e., from the back to the front in front of the eye contralateral to the recording side. Because the H1 neuron connects both lobula plates to one other, all recordings were done from the axon of the cell. The pattern consisted of a sine wave grating presented on a computer monitor (32 cm × 24 cm; Dell, Round Rock, TX) 14 cm in front of the fly by means of a graphics board and custom written software (DELPHI, Borland, Scotts Valley, CA) at a frame rate of 100 Hz. As seen by the fly, the stimulus covered a spatial angle of ≈4 steradian. The mean luminance was varied by means of neutral density filters placed between the fly and the monitor. For each stimulus condition, 10 sweeps of identical stimuli were presented. Spikes were recorded extracellularly with a tungsten electrode inserted in the lobula plate, fed through a threshold device, and transferred at a 1-kHz temporal resolution to a computer (Pentium II-based PC with a DAS16 I/O board from Metrabyte, Tauton, MA). The stimulation software was written in DELPHI. The response was quantified as the difference in spike rates between stimulation and rest. The resting rate was as determined during the last second before stimulus onset. Response values were normalized for each fly to the maximum response obtained under a particular stimulus condition.

Results

Pattern Dependence of the Local Detector Signals. In a first series of experiments, we measured local [Ca^{2+}] dynamics in small dendritic branches of lobula plate tangential cells, together with axonal membrane potential, while stimulating the fly with a drifting grating at mean luminance levels varying from 50 to 50,000 cd/m^2. A schematic of our setup using 2-photon excitation together with the stimulus device is shown in Fig. 3. In Fig. 2*b*, grating motion along the preferred direction of a tangential cell of the vertical system (VS2 cell, Fig. 2*d*) leads to a tonic elevation of the dendritic [Ca^{2+}] signal with a superimposed periodic modulation. The tonic response comprised a 50% change of fluorescence in this cell (all responses given as changes of fluorescence relative to the resting level). The AC component had a frequency of 1.3 Hz and was phase-locked to the pattern motion. When the pattern moved at twice or at half that velocity, modulations occurred at 2.6 Hz or 0.65 Hz, respectively (data not shown). For the stimulus parameters chosen here, the amplitude of the AC component was ≈20% of the DC response. In Fig. 2*c*, where the axonal membrane potential is displayed, the neuron fires a barrage of small-amplitude spikes and is slightly depolarized (30, 31). Unlike the optical signal, the electrical signal contains no apparent AC component.

We conducted these experiments on cells in the horizontal system (HSN and HSE cells) and in the vertical system (VS1–4) in a total of 11 flies. Optical recordings were obtained from one small dendritic branchlet while stimulating the fly with the grating drifting along the preferred direction of the cell at four different mean luminance levels. With increasing mean luminance, the modulation amplitude increased, with a pronounced saturation characteristic, from ≈5% at low levels to ≈25–30% at high levels (Fig. 4*a*, filled circles). As is also expected from the Reichardt model, the DC level generally increased with mean luminance but occasionally declined toward the highest mean luminance level in some of the experiments (Fig. 4*a*, filled squares). In Fig. 4*b*, the average electrical response, recorded from the axon of these cells, is shown as a function of the mean luminance. Like the DC [Ca^{2+}] signal, the membrane depolarization increased slightly with increasing mean luminance and saturated toward higher values with a slight decline at the highest luminance level. In summary, the lack of any

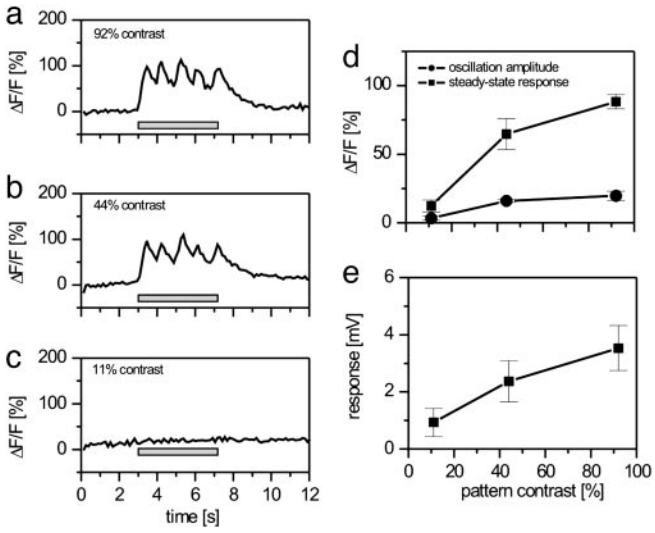

Fig. 5. Contrast dependence of motion responses. (*a–c*) Examples of the local [Ca^{2+}] response of a VS cell during preferred direction motion using three different stimulus contrasts. (*d*) Oscillation amplitude and steady-state [Ca^{2+}] signal as a function of stimulus contrast. (*e*) Average membrane depolarization during preferred direction motion is shown as a function of stimulus contrast. Values represent the mean ± SEM from measurements on four different flies.

reduction in the amplitude of the dendritic modulations of [Ca^{2+}] with increasing mean luminance strongly favors the Reichardt detector hypothesis over a gradient motion detector mechanism throughout the entire luminance range of the fly visual system.

Because the SNR also depends on the contrast of the stimulus, we next measured the effect of stimulus contrast on dendritic modulations of [Ca^{2+}]. With a mean luminance level of 5,000 cd/m^2, we used stimulus contrast values of 11%, 44%, and 92% while keeping all other stimulus parameters identical to those used in the previous set of experiments. We measured [Ca^{2+}] and electrical responses in two horizontal and two vertical cells in a total of four animals. In Fig. 5 *a–c*, the dendritic [Ca^{2+}] from one such experiment is plotted for the three stimulus contrast values. At high and intermediate contrast conditions, [Ca^{2+}] showed clear DC and AC signals, again at the temporal frequency of and phase-locked to the stimulus. At low contrasts, i.e., 11% (Fig. 5*c*), neither a DC signal nor a modulation was detectable in this cell. This qualitative statement also applies for the average result from all experiments (Fig. 5*d*): At 44% and 92% contrast we found a large DC signal and significant modulations in dendritic [Ca^{2+}], whereas at 11% contrast, such signals were rather small. This differs from the electrical response (Fig. 5*e*), which, like the [Ca^{2+}] signal, increased with increasing contrast and had a small but significant amplitude at 11% contrast. This discrepancy between electrical signal and cytosolic calcium is due to the activation characteristics of the calcium current in these cells, which is only beginning to rise slightly above the resting potential (14). Most important, however, with respect to the Reichardt detector hypothesis, is the fact that no decrease in the amplitude of the dendritic [Ca^{2+}] modulation was found with increasing SNR. Instead, [Ca^{2+}] modulations increased with increasing stimulus contrast.

Pattern Dependence of the Integrated Detector Output. Another prediction of the Reichardt model is that the velocity optimum of the spatially integrated output of an array of such detectors, the global signal, should depend on the spatial pattern wavelength in such a way that the ratio of wavelength and speed (and hence the temporal modulation frequency) remains constant. In contrast, the gradient detector predicts no such dependence of the global signal

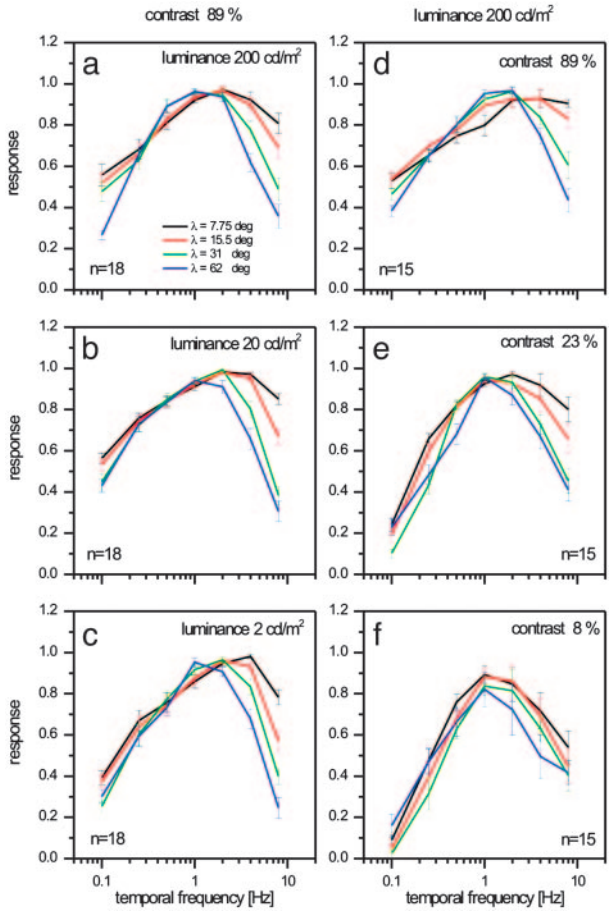

Fig. 6. Temporal frequency tuning of the H1 neuron for different grating wavelengths λ measured at different luminance levels (*a–c*) and pattern contrasts (*d–f*). In the experiments shown in *a–c*, the pattern contrast was 89%. In the experiments shown in *d–f*, the pattern luminance was 200 cd/m^2. At each luminance and contrast level, the optimum temporal frequency is clearly seen to remain constant, irrespective of the spatial wavelength of the grating. Values represent the mean ± SEM from measurements on 18 (*a–c*) and 15 (*d–f*) different flies. For each fly and each luminance or contrast condition, responses were normalized to the maximum response.

on the pattern wavelength. To decide between these alternative predictions at various SNR levels, we conducted two sets of experiments, again covering a range of conditions that result in widely varying SNRs. We measured the pattern dependence of the velocity optimum with different levels of stimulus luminance and contrast.

In Fig. 6 *a–c*, responses of the motion-sensitive H1 neuron are shown for four different pattern wavelengths, all presented at 89% stimulus contrast at three different mean luminance levels. The response is plotted as a function of the temporal frequency. It is obvious from the results that the response curves essentially overlay and peak at the same temporal frequency of ≈1 Hz, irrespective of pattern wavelengths and, hence, of the absolute pattern velocity. Most notably, this is as true for low luminance levels as it is for high luminance levels. The temporal frequency optimum of ≈1 Hz in all tested pattern wavelengths is independent of luminance.

In the next series of experiments (Fig. 6 *d–f*), we kept the mean luminance at a level of 200 cd/m^2 and measured the pattern-wavelength dependence at different pattern contrasts (89%, 23%, and 8%). Again, for all three contrast values tested, the response curves overlay and peak at the same temporal frequency, irrespective of pattern wavelengths and, hence, of the absolute pattern velocity. There are, however, slight differences between the response curves at high and low contrast values (compare Fig. 6 *d* and *f*): At low stimulus contrasts, the curves fall off more steeply toward smaller frequencies than they do at high stimulus contrasts where the response curves are, in general, flatter. Most important in the present context, however, is that for different pattern wavelengths, the response optimum remains at the same temporal frequency and not at the same velocity.

In summary, these experiments demonstrate that the pattern dependence of the spatially integrated motion signal persists despite large changes in the SNR at the input to the detection system. We find the velocity optima to scale with spatial pattern wavelength at all luminance levels and at all stimulus contrasts tested, resulting in a constant temporal frequency optimum. As in the measurements of local [Ca^{2+}] signals, we find no indication that the algorithm used in the motion processing pathway changes with changing SNR.

Discussion

The goal of this study was to test whether a shift occurs in the fly motion detection algorithm from a Reichardt detector to a gradient detector when going from low to high SNRs (13). We addressed this question by measuring the pattern, luminance, and contrast dependencies of local [Ca^{2+}] signals in large-field motion-sensitive neurons of the fly lobula plate and of the H1 neuron's firing rate in response to drifting gratings. One difficulty is in estimating precisely how large the actual SNR levels were under the various luminance and contrast values used in these experiments. Following the calculations of Grewe *et al.* (32), a mean luminance level of 1 cd/m^2 results in ≈1 photon per photoreceptor per ms in the blowfly eye. Given that the arrival of photons is a Poisson process wherein the variance equals the mean luminance (in photon units), the shot-noise-limited SNR grows with the square root of the mean luminance. A photoreceptor integration time of 10 ms would yield SNR levels ranging from ≈4 (at 2 cd/m^2) up to 700 (at 50,000 cd/m^2) in the experiments described above. Whereas the luminance values used in the first experiment (Fig. 4) indeed cover the maximum light intensities experienced outdoors on a sunny day (≥10,000 cd/m^2; refs. 33 and 34), the maximum mean luminance values used in the second experiment (Fig. 6) reached only 200 cd/m^2, which corresponds more closely to conditions at sunset than at noon (33). On the other hand, given that internal pupil mechanisms limit the maximum photoconversion rate in fly photoreceptors to ≈10^6/s (35), luminance levels >1,000 cd/m2 should lead to a strong saturation in the response. We are confident, therefore, that the luminance levels tested, in particular in the first experiment, cover whatever the fly will experience when flying outdoors. As for the contrast, the SNR level at the input should scale linearly with the pattern contrast when considering peak-to-peak measurements. Further quantification of this point, however, is complicated because the local light level *per se*, or its modulation, is not the stimulus signal: Motion detection requires a comparison between the phase of such modulations in neighboring image locations, and the exact stimulus cannot be defined without defining the processing mechanism.

Nevertheless, our findings on the local detector signals demonstrate that the signal characteristics do not change when the SNR in the stimulus is varied by using widely different mean luminances and stimulus contrasts. These conclusions are based on measurements of cytosolic [Ca^{2+}], which qualifies as a reliable reporter of neural activity in these cells (14–18). Therefore, the temporal modulation in [Ca^{2+}] reflects the temporal modulations of the activity of local motion-sensing elements and demonstrates the pattern dependence of local motion sensing. Collateral excitation by the fluorescence excitation light, which is unavoidable in conventional 1-photon fluorescence microscopy, does not occur from the infrared laser used for 2-photon excitation because the infrared laser beam is invisible to the fly's photoreceptors.

In addition to the obvious dependence of the local oscillatory component on the stimulation pattern, there is the more subtle

dependence of the velocity optimum on the pattern that survives spatial and temporal averaging. For time- or space-averaged responses to gratings drifting at constant velocity, the Reichardt model predicts that the optimum response should occur at a constant ratio of the velocity and grating wavelength. This prediction was confirmed in numerous psychophysical studies in humans (refs. 36–41; for a review see ref. 4) and in insects (for a review see ref. 42). In particular, the optomotor response of flies (22, 23, 43) and recordings from the motion-sensitive interneurons H1 (44) provided strong evidence that the velocity optimum indeed shifts as predicted with the wavelength of the pattern. Whereas most of these studies used low light levels with , presumably, low SNRs, pattern dependency was also found in *Drosophila* optomotor behavior at high mean luminance levels of ≈320 cd/m^2 and a pattern contrast of 100% (24). Those stimulus parameters assured a high SNR level and, therefore, provide an argument against the gradient motion detector being used in its supposed domain of excellence, the high SNR regime. The mean luminances used in our experiments on the H1 neuron ranged from 2 to 200 cd/m^2. The clear dependence on temporal frequency rather than on absolute velocity with different wavelengths (Fig. 6 *a–c*) at all luminance levels again provides strong support for the Reichardt detector at all SNRs.

In addition to purely theoretical arguments about optimal motion detection (13), there are two sets of experimental results that appear to support the presence of gradient-based motion detection at high SNRs. One observation is that, contrary to the prediction of the Reichardt model, which calls for the signal amplitude to increase quadratically with the stimulus contrast, the amplitudes become contrast-independent at high contrast levels. For example, in flies, a quadratic contrast dependency is found only for small contrast levels, up to ≈5–10% (e.g., figure 7 of ref. 24, optomotor response of *Drosophila*, mean luminance = 16 cd/m^2; figure 10 of ref. 22, optomotor response of *Musca*, mean luminance = 110 cd/m^2; and figure 2 of ref. 45, optomotor response of *Drosophila*, mean luminance = 300 cd/m^2). For higher contrast values the response becomes largely contrast-independent (22, 23, 45, 46). In humans it has been found that low-contrast gratings are perceived to be slower than high-contrast gratings moving at the same velocity (47–49). Whereas contrast independence is exactly the behavior one would expect from a gradient detector (contrast effects are cancelled out by temporal and spatial gradient ratios), alternatively, contrast independence could result from a saturating nonlinearity (46) or a contrast adaptation (50) elsewhere in the visual pathway. This interpretation is favored by our observation that, even at high contrasts, where we do see the response amplitudes becoming contrast-independent, the characteristic spatial frequency/velocity optimum still exists, inconsistent with the gradient detector model (Fig. 6*a*).

Another observation in apparent support of a gradient detector concerns the free-flight performance of honey bees. In a series of experiments, Srinivasan and colleagues (51, 52) demonstrated that honey bees flying freely through a tunnel covered with vertical grating patterns do not rely on the temporal frequency in their response, but rather on the image velocity, irrespective of the spatial wavelength. Although these results cannot be explained readily by the Reichardt model of motion detection, they are not necessarily in favor of the gradient detector either (53). First, the dependence on temporal frequency rather than on image velocity only holds for the response optima under steady conditions. Whereas these conditions are hardly met in free flight, under transient conditions, Reichardt detectors show a completely different behavior that, so far, has only been studied by using a small subset of stimulus parameters (46). Second, as a more general argument, the actual properties of a sensor cannot be extracted readily from the behavior under closed-loop conditions where, in addition to the properties of the sensor, the dynamics of the control system also come into play.

In summary, our findings demonstrate that both local and global motion signals are pattern-dependent whether the stimulus has low or high SNRs. This finding argues strongly in favor of the Reichardt detector under all stimulus conditions and against an SNR-dependent switchover between processing schemes.

We thank Renate Gleich for technical assistance in the experiments shown in Fig. 6. This work was supported by the Max Planck Society.

1. Hassenstein, B. & Reichardt, W. (1956) *Z. Naturforsch.* **11b,** 513–524.
2. Reichardt, W. (1961) in *Sensory Communication*, ed. Rosenblith, W. A. (MIT Press/Wiley, New York), pp. 303–317.
3. Reichardt, W. (1987) *J. Comp. Physiol. A* **161,** 533–547.
4. Borst, A. & Egelhaaf, M. (1989) *Trends Neurosci.* **12,** 297–306.
5. Egelhaaf, M. & Reichardt, W. (1987) *Biol. Cybern.* **56,** 69–87.
6. Adelson, E. H. & Bergen, J. R. (1985) *J. Opt. Soc. Am. A* **2,** 284–299.
7. van Santen, J. P. H. & Sperling, G. (1985) *J. Opt. Soc. Am. A* **2,** 300–320.
8. Borst, A. & Egelhaaf, M. (1993) in *Visual Motion and Its Role in the Stabilization of Gaze*, eds. Miles, F. A. & Wallman, J. (Elsevier, New York), pp. 3–27.
9. Limb, J. O. & Murphy, J. A. (1975) *Comput. Graphics Image Processing* **4,** 311–327.
10. Fennema, C. L. & Thompson, W. B. (1979) *Comput. Graphics Image Processing* **9,** 301–315.
11. Hildreth, E. & Koch, C. (1987) *Annu. Rev. Neurosci.* **10,** 477–533.
12. Srinivasan, M. V. (1990) *Biol. Cybern.* **63,** 421–443.
13. Potters, M. & Bialek, W. (1994) *J. Physiol. (Paris)* **4,** 1755–1775.
14. Oertner, T. G., Brotz, T. & Borst, A. (2001) *J. Neurophysiol.* **85,** 439–447.
15. Haag, J. & Borst, A. (2000) *J. Neurophysiol.* **83,** 1039–1051.
16. Borst, A. & Single, S. (2000) *Neurosci. Lett.* **285,** 123–126.
17. Single, S. & Borst, A. (2002) *J. Neurophysiol.* **87,** 1616–1624.
18. Brotz, T. & Borst, A. (1996) *J. Neurophysiol.* **76,** 1786–1799.
19. Single, S. & Borst, A. (1998) *Science* **281,** 1848–1850.
20. Borst, A. & Single, S. (1999) in *Imaging Living Cells: A Laboratory Manual*, eds. Yuste, R., Lanni, F. & Konnerth, A. (Cold Spring Harbor Lab. Press, Woodbury, NY), Chap. 44.
21. Denk, W. & Svoboda, K. (1997) *Neuron* **18,** 351–357.
22. Fermi, G. & Reichardt, W. (1963) *Kybernetik* **2,** 15–28.
23. Buchner, E. (1976) *Biol. Cybern.* **24,** 85–101.
24. Götz, K. G. (1964) *Kybernetik* **2,** 77–92.
25. Denk, W., Strickler, J. H. & Webb, W. W. (1990) *Science* **248,** 73–76.
26. Denk, W. & Detwiler, P. B. (1999) *Proc. Natl. Acad. Sci. USA* **96,** 7035–7040.
27. Euler, T., Detwiler, P. B. & Denk, W. (2002) *Nature* **418,** 845–852.
28. Hardie, R. C. (1979) *J. Comp. Physiol.* **129,** 19–33.
29. Denk, W. (2004) in *Imaging Living Cells: A Laboratory Manual*, eds. Yuste, R., Lanni, F. & Konnerth, A. (Cold Spring Harbor Lab. Press, Woodbury, NY), 2nd Ed., in press.
30. Hengstenberg, R. (1977) *Nature* **270,** 338–340.
31. Haag, J. & Borst, A. (1996) *Nature* **379,** 639–641.
32. Grewe, J., Kretzberg, J., Warzecha, A. & Egelhaaf, M. (2003) *J. Neurosci.* **23,** 10776–10783.
33. Egelhaaf, M., Grewe, J., Kern, R. & Warzecha, A. K. (2001) *Vision Res.* **41,** 3627–3637.
34. Lewen, G. D., Bialek, W. & de Ruyter van Steveninck, R. R. (2001) *Network* **12,** 317–329.
35. Howard, J., Blakeslee, B. & Laughlin, S. B. (1987) *Proc. R. Soc. London Ser. B* **231,** 415–435.
36. Watanabe, A., Mori, T., Nagata, S. & Hiwatachi, K. (1968) *Vision Res.* **8,** 1245–1263.
37. Tolhurst, D. J., Sharpe, C. R. & Hart, G. (1973) *Vision Res.* **13,** 2545–2555.
38. Pantle, A. (1974) *Vision Res.* **14,** 1229–1236.
39. Kelly, D. H. (1979) *J. Opt. Soc. Am.* **69,** 1340–1349.
40. Burr, D. C. & Ross, J. (1982) *Vision Res.* **22,** 479–484.
41. Wright, M. J. & Johnston, A. (1985) *Vision Res.* **25,** 1947–1955.
42. Egelhaaf, M. & Borst, A. (1993) in *Visual Motion and Its Role in the Stabilization of Gaze*, eds. Miles, F. A. & Wallman, J. (Elsevier, New York), pp. 53–77.
43. Eckert, H. (1973) *Kybernetik* **14,** 1–23.
44. Eckert, H. (1980) *J. Comp. Physiol.* **135,** 29–39.
45. Hengstenberg, R. & Götz, K. G. (1967) *Kybernetik* **3,** 276–285.
46. Egelhaaf, M. & Borst, A. (1989) *J. Opt. Soc. Am. A* **6,** 116–127, erratum (1990) **7,** 172.
47. Thompson, P. (1982) *Vision Res.* **22,** 377–380.
48. Blakemore, M. R. & Snowden, R. J. (1999) *Perception* **28,** 33–48.
49. Anstis, S. (2001) *Perception* **30,** 785–794.
50. Harris, R. A., O'Carroll, D. C. & Laughlin, S. B. (2000) *Neuron* **28,** 595–606.
51. Kirchner, W. H. & Srinivasan, M. V. (1989) *Naturwissenschaften* **76,** 281–282.
52. Srinivasan, M. V., Lehrer, M., Kirchner, W. H. & Zhang, S. W. (1991) *Visual Neurosci.* **6,** 519–535.
53. Egelhaaf, M. & Borst, A. (1992) *Naturwissenschaften* **79,** 221–223.